Corrosion Behavior of Zinc-Aluminum-Magnesium Coated Steel in Simulated Marine Atmosphere

Tianzhen Gu[1,2], Peng Zhang[3,4], Mingxiao Guo[1,2], Can Peng[1,2], Cheng Ma[4], Yuwei Liu[1,],*
Zhenyao Wang[1,]*

[1] Institute of Metal Research, Chinese Academy of Sciences, Shenyang 110016, China
[2] School of Materials Science and Engineering, University of Science and Technology of China, Shenyang 110016, China
[3] National Engineering Laboratory of Advanced Coating Technology for Materials, China Iron & Steel Research Institute Group, Beijing 100081, China
[4] HBIS Group Technology Research Institute, Shijiazhuang 050023, China
[*]E–mail: ywliu12s@imr.ac.cn; zhywang@imr.ac.cn

The corrosion behavior of zinc-aluminum-magnesium (ZAM) coated steel in a simulated marine atmosphere was investigated using compositional, morphological, electrochemical, and mass loss analyses. The results revealed that the corrosion rate of ZAM coated steel fluctuated because of the corrosion products formed during its exposure to the marine atmosphere, and the mass loss after 1848 h of exposure was 27.37 g·m^{-2} after 1848 hours' exposure. The corrosion preferentially occurred in the eutectic phases, especially in the eutectic phases near the primary zinc phase and with an area smaller than the primary zinc phase. As the exposure time increased, some of the corrosion products flaked off from the coating, leading to the aggravation of local corrosion and the formation of corrosion pits. Moreover, the corrosion products in the corrosion pits were dissolved, which can be attributed to the decrease in pH caused by the consumption of hydroxides during the chemical reactions of the corrosion process.

1. INTRODUCTION

The structural steel coated by galvanized coatings is widely used for home appliance and automotive applications. The elements of Al, Mg, Si were added to coatings in order to increase corrosion resistance and satisfy the requirements of manufacturing. ZAM coating, a novel coating developed from galvanized coating, has an excellent corrosion resistance and is being used in buildings,

households, and the automotive industry[1–4]. Because of their lightweight design, ZAM coatings would have widespread applications. Tomas Prosek evaluated the corrosion characteristics of ZAM using an accelerated cyclic corrosion test and found that compared with the thickness of a traditional hot–dip galvanized coating, the thickness of the ZAM coating may be reduced by 2–3 times with the same corrosion resistance[5].

Atmospheric corrosion occurs in ZAM coated steel when it is used in outdoor environments. Therefore, the atmospheric corrosion mechanism of ZAM coated steel must be investigated. Because of their Al and Mg contents, ZAM coatings have several phases, such as the primary zinc phase, ternary Al–Zn–MgZn2 eutectic phase, binary Zn–Al eutectic phase, and $MgZn_2$–Zn phase, complicating the corrosion process that takes place in the coatings[6–8]. The corrosion that occurred in these coatings is selective and not uniform, $MgZn_2$ in the Mg–rich eutectic phase corroded preferentially[7–11]. Volovitch[12] studied ZAM coatings subjected to NaCl spray testing. They found that Zn and Mg preferentially dissolved during the early stages of corrosion. Thierry and coworkers[13] studied ZAM coated steel subjected to outdoor exposure for 4 years and found that the eutectic phases suffered from corrosion more than the zinc–rich phases. The coatings had penetrated the steel substrate after six months of outdoor exposure because of pitting corrosion. Therefore, the pitting corrosion mechanism of ZAM coatings also needs to be investigated.

Because outdoor exposure experiments require considerable time and resources, researchers typically conduct indoor simulation experiments to explore the atmospheric corrosion in materials, especially in corrosion–resistant materials[12,14–18]. Pollutants, the time of wetting, and temperature are the main factors that affect the atmospheric corrosion of materials[14,24]. The marine atmosphere is a typical corrosive environment. Chloride ions have a significant effect on marine atmospheric corrosion. Therefore, in this study, the corrosion behavior of ZAM coated steel in a simulated marine atmosphere was investigated. The study would provide a reference for the application of ZAM coated steel in a marine atmosphere and contribute to the knowledge of the corrosion process of ZAM coated steel in a marine atmosphere.

2. METHODS

2.1 Materials and samples preparation

The ZAM coated steel used in the study had a thickness of approximately 23 μm (275 $g \cdot m^{-2}$) and was supplied by HBIS GROUP; its mass percent chemical composition was 3.4 Mg, 5.6 Al, and 81.5 Zn (other elements were not detected).

The X–ray diffraction (XRD) diagram of ZAM coated steel before corrosion is shown in Fig.1 (a), which consists of η–Zn (P63/mmc), α–Al (Fm–3m) and $MgZn_2$ (P63/mmc). In Fig.1 (b), the white circular site represents the primary zinc phase, and pinstripes mark the ternary Al–Zn–$MgZn_2$ eutectic phase; thick stripes mark the binary Zn–Al eutectic phase. The compositions of different phases detected from Energy Dispersive Spectroscopy (EDS) analysis are shown in Table 1. The proportion of primary zinc phase is approximately 60% according to the cross–sectional morphology of ZAM before corrosion.
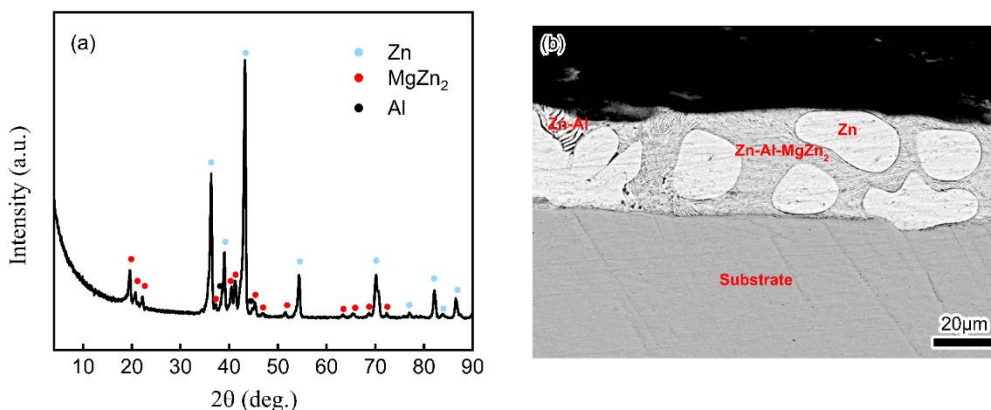
Figure 1. (a) The phase composition and (b) cross–sectional morphology of ZAM before corrosion

Table 1. The element composition of different phases of ZAM

Phase	Element (wt %)		
	Zn	Al	Mg
Zn	96.22	3.78	—
Zn–Al	92.14	7.86	—
Zn–Al–MgZn$_2$	82.74	13.84	3.42

Four parallel specimens were cut into 100×50 mm pieces for use in the cyclic accelerated corrosion test conducted for each period, and the edges of the specimens were covered with an adhesive tape to prevent cut–edge corrosion from occurring. All the samples were cleaned with acetone and alcohol before being used. After retrieving the corroded samples, three specimens were prepared for mass loss measurements and one for electrochemical, compositional, and corrosion morphology analysis. The sample used for the electrochemical measurements was wired with a copper conductor and then sealed with the polytetrafluoroethylene tape and rosin paraffin, leaving a measuring area of 1 cm^2. The sample used for the cross–sectional morphology analysis was embedded in the epoxy resin. It was polished after being wet–ground to 2000 grade using the silicon carbide abrasive paper. The samples were then sprayed with carbon before they were observed using a scanning electron microscope equipped with an energy dispersive spectrometer.

2.2 Cyclic accelerated corrosion test

The accelerated corrosion test was conducted in a Q–Fog salt–spray test chamber using a 5 wt% NaCl solution as the corrosion medium to simulate the marine atmosphere. The test was performed at a constant temperature of 35 °C, and the cycle procedure was as follows: (1) spray 2 h, (2) dry 4 h, (3) humid 1 h, (4) dry 2 h, (5) repeat (3) and (4) once. The corroded samples were retrieved after 168, 336,

504, 672, 840, and 1848 h.

2.3 Mass loss measurements

For the mass loss analysis, the tapes and nonadherent corrosion products were removed, and the corroded samples were immersed in a saturated solution of glycine at room temperature for 1–10 minutes in accordance with ISO 8407. All corrosion products present were thereafter removed, rinsed with deionized water, dehydrated with alcohol, dried using an air dryer, stored in a desiccator for 24 h, and finally weighed using an analytical balance.

2.4 Electrochemical measurements

The electrochemical measurements were conducted at room temperature in a 0.1mol/L NaCl solution after potential stabilize using a PARSTAT Model 2273 controlled by Powersuite® software. A conventional three–electrode electrochemical cell containing a saturated calomel electrode as the reference electrode, a platinum counter electrode, and a working electrode, was used in the measurements.

Electrochemical impedance spectroscopy (EIS) measurements were fixed with an alternating current amplitude of open circuit voltage 10 mV between 100 kHz and 10 mHz. The EIS data were fitted using the Zsimpwin software. Linear polarization resistance measurements were conducted with a sweep rate of 0.3333 mV/s and a sweep range of ±10 mV (vs. OCP). Potentiodynamic polarization measurements were conducted with a sweep rate of 0.3333 mV/s and a sweep range of –0.25 V (vs. OCP)–0.3 V (vs. OCP). All electrochemical measurements were conducted at least thrice to ensure reproducibility.

2.5 Morphology and composition

After corrosion, the cross–sectional morphology and chemical composition of the samples were analyzed using an ESEM XL30 FEG scanning electron microscopy and energy dispersive spectrometer, respectively. The corrosion products were determined using an XPERT–PRO X–ray diffractometer with a Cu target. The electrical parameters were 40 KV, 40 mA and $2\theta = 4°–90°$. The angle of incidence was 0.5°.

3. RESULTS AND DISCUSSION

3.1 Mass loss measurements

The mass loss of ZAM in the simulated marine atmosphere is shown in Fig.2 (a) for different time. The mass loss gradually increased as the corrosion progressed. The material corrosion rate obtained by mass loss analysis can be used to determine corrosion regulation. The corrosion rate can be described

as:

$$V_n = \frac{D_n - D_{n-1}}{t_n - t_{n-1}} \tag{1}$$

Where V_n is the corrosion rate (g·m^{-2}·h^{-1}), t is the time (h), D is the mass loss per unit area (g·m^{-2}) and n is the number of the period, in this paper, for example, 0–168 h was the first period as $n = 1$. Fig.2 (b) shows the corrosion rate of ZAM in the simulated marine atmosphere at different corrosion time. The corrosion rate of ZAM coated steel varied and fluctuated, and the curve was shaped like the letter W. The corrosion rate firstly declined at 168–336 h, then increased gradually at 336–672 h. Afterward, it exhibited a sharp decline at 672–840 h, and started to increase again at the end stage. The average corrosion rate reached its maximum at the end stage.
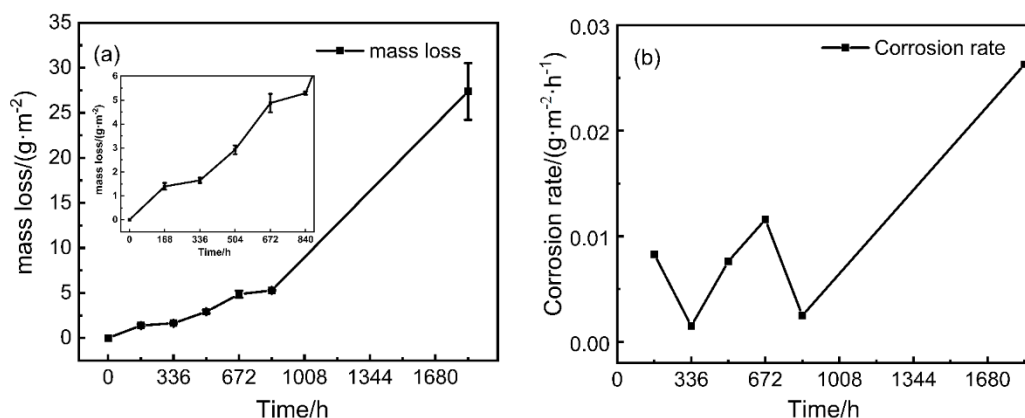

Figure 2. (a) Mass loss and (b) corrosion rate of ZAM in the simulated marine atmosphere at different time

3.2 Composition

Fig.3 (a) shows the XRD results of ZAM coated steel after different corrosion time. Only one corrosion product, namely, $Zn_5(OH)_8Cl_2·H_2O$ was detected, and no corrosion products containing Al and Mg were detected. The $MgZn_2$ and Zn peaks declined unobtrusively during the early stages of corrosion, and their changes became obvious at the latter stages. The change in the peak intensity of Al was not obvious throughout the entire corrosion process, probably because Al remained on the coating in an insoluble form during the early stages of corrosion[12]. Throughout its entire period of exposure, it exhibited only slight corrosion. The corrosion product containing Mg might have been dissolved and washed away[13]. Interestingly, the $Zn_5(OH)_8Cl_2·H_2O$ peaks at 168 h, which were particularly distinct, disappeared suddenly at 336 h. After that, they gradually increased with the increasing exposure time. Because $Zn_5(OH)_8Cl_2·H_2O$ was a protective corrosion product[12,22], the generation of large amounts of it at 168 h would had inhibited corrosion and reduced the corrosion rate. Therefore, the corrosion rate at 168–336 h was much lower than that of 0–168 h. Abnormally, the peaks of Zn at 504 h were stronger than those at 672 h as shown in Fig.3 (b), and the reason for it was discussed below.
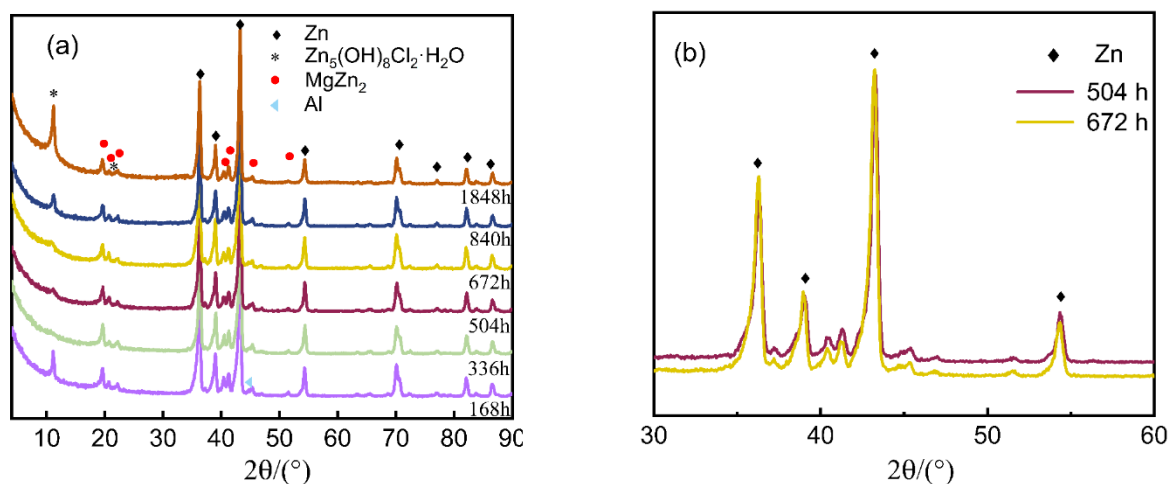
Figure 3. X–ray diffraction diagrams of ZAM coated steel in the simulated marine atmosphere at different time

3.3 Cross–sectional of corrosion product morphology

Fig.4 (a) displays the cross–sectional morphology of the corrosion products presented in the ZAM coated steel after 168 h. The outer layer above the coating was discontinuous and was separated from the coating. The element composition of the outer layer at the marked site is presented in Table 2. Elements O and Cl were detected in the outer layer, indicating that the outer layer of the coating was the corrosion products. The volume expanded as the corrosion progressed, causing some of the corrosion products to rupture, which might be the reason inducing the corrosion products discontinuous. Meanwhile, the binding force between ZAM coating and discontinuous corrosion products was poor, the latter could easily flake out from the coating. Therefore, the $Zn_5(OH)_8Cl_2·H_2O$ peak was almost absent at 336 h in the XRD results. Combining with the results of the corrosion rate of 0–168 h and 168– 336 h, it can be speculated that the corrosion resistance of $Zn_5(OH)_8Cl_2·H_2O$ was stronger than that of ZAM coating and the formation of $Zn_5(OH)_8Cl_2·H_2O$ above the coating could hinder further corrosion to some extent.

A corrosion pit was found at 504 h as shown in Fig.4 (b) and the corrosion products in the corrosion pit almost disappeared. Fig.4 (c) displays the cross–sectional morphology of the corrosion products on the ZAM coated steel after 840 h. From Fig.4 (b) and (c), the eutectic phases, especially those near the primary zinc phase and smaller in area than the primary zinc phase, were preferentially corroded. At the interface between the primary zinc and eutectic phases, the potential of the primary zinc phase was lower than that of the eutectic phase, thus the primary zinc phase would have acted as the cathode and the eutectic phase as the anode during the electrochemical reaction. The corrosion site was large cathode and small anode as shown in Fig.4 (b) and (c). The corrosion of eutectic phases in these sites was more severe than the corrosion in large area eutectic phases, such as site A shown in Fig.4 (a). Accordingly, there was more serious corrosion happening as corrosion time prolonged.

Fig.4 (d) and (e) display the cross–sectional morphology of the corrosion products present in the ZAM coated steel after 1848 h. As shown in Fig.4 (d), corrosion products appeared in the eutectic phase

near the primary zinc phase and the primary zinc phase was surrounded by corrosion products. Both the eutectic phase and primary zinc phase in site D were corroded more severely than those at other sites. As shown in Fig.4 (e), the corrosion in the large area eutectic phase was uniform, the coatings surface was uneven and the primary zinc phase was bulged.
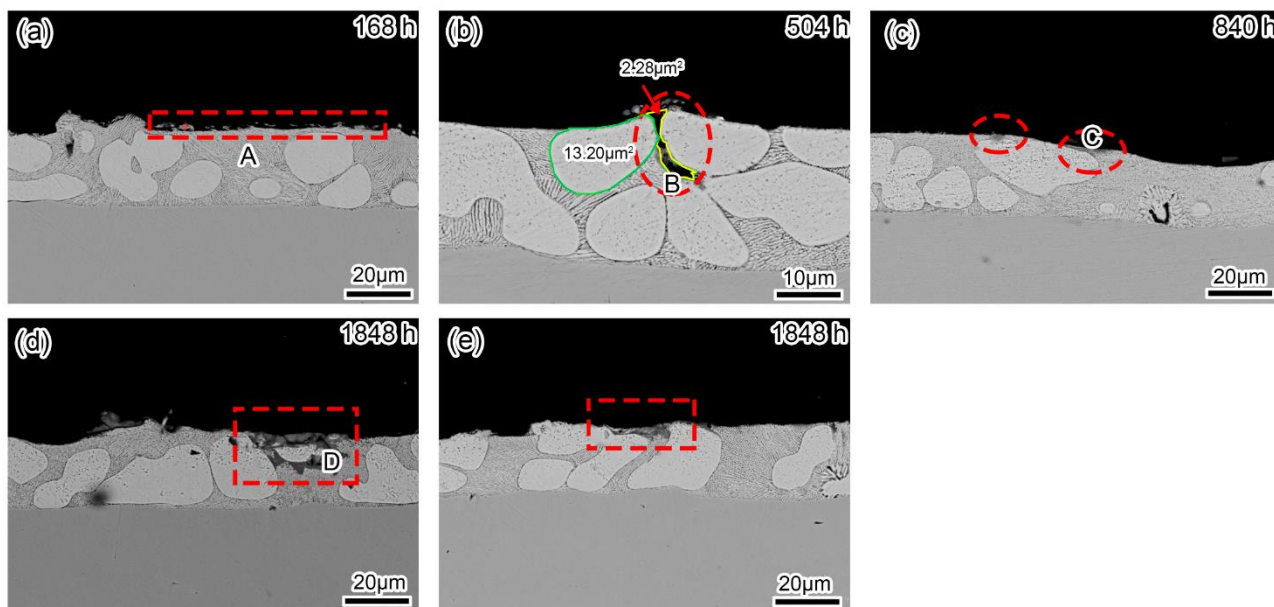

Figure 4. The cross–sectional morphology of corrosion products on ZAM coated steel in the simulated marine atmosphere at different time: (a) 168 h; (b) 504 h; (c) 840 h; (d) and (e) 1848 h.

Table 2. The element composition of outer layer of ZAM at 168 h

Elements	Zn	O	Mg	Al	Si	Cl
（At%）	72.03	9.94	1.41	12.53	3.05	1.04

3.4 Electrochemical measurements

3.4.1 Polarization measurements results

Fig.5 shows the potentiodynamic and linear polarization curves of ZAM exposed to the simulated marine atmosphere at different corrosion time. According to the Stern formula:

$$I_{corr} = \frac{B}{R_p} = \frac{\beta_c \beta_a}{\beta_c + \beta_a} \cdot \frac{1}{R_p} \qquad (2)$$

Where R_p is polarization resistance fitted from the linear polarization curves, and β_a and β_c are the anode and cathode Tafel slope, respectively, fitted from the potentiodynamic polarization curves. The variation of both calculated corrosion current (I_{corr}^*) and fitted corrosion current (I_{corr}) with corrosion time are shown in Fig.6, the variation patterns of both the fitted and the calculated I_{corr} are similar. Both declined first and then increased at 168–504 h. They started to decline again at 672 h and then started to

increase at 840 h. They started to decline again at 1848 h. The polarization results were also consistent with the corrosion rate regulation (they were shaped like the letter W at colored part). The cathodic kinetics were dominated by oxygen reduction, which varied as the corrosion products built up.
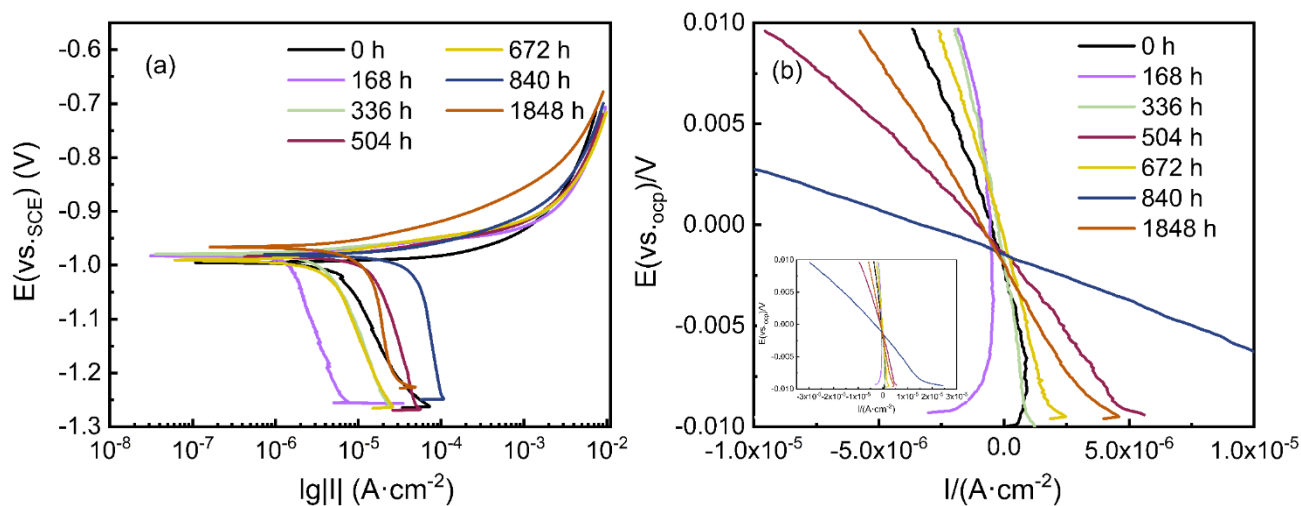

Figure 5. (a) Potentiodynamic curves and (b) linear polarization curves of ZAM in the simulated marine atmosphere at different corrosion time
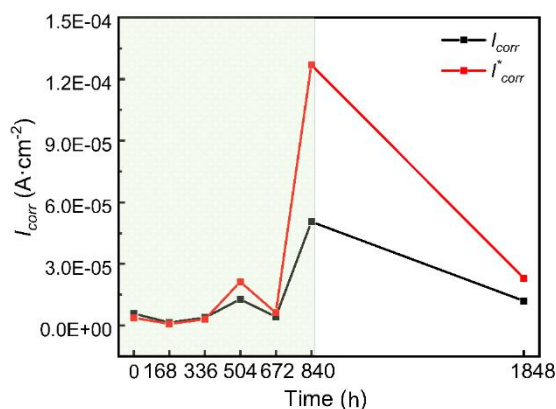

Figure 6. Evolutions in I_{corr} and I_{corr}^{*} of ZAM in the simulated marine atmosphere at different corrosion time

3.4.2 EIS results

Fig.7 shows the electrochemical impedance spectrum of ZAM exposed to the simulated marine atmosphere at different corrosion time. As shown in Fig.7 (a), two capacitive reactance arcs were present in the Nyquist diagrams of all stages of corrosion. Inductive loops were observed at high frequencies at 336 and 504 h, which indicated local corrosion. The capacitive reactance arcs of 168 h were much larger than others, which indicated that the corrosion products had high corrosion resistance after the ZAM

coatings were corroded for 168 h. Corrosion products can effectively inhibit the corrosion process and reduce the decline of the corrosion rate at 168–336 h.

The Bode–phase diagram of the samples are shown in Fig.7 (b), which indicate two time constants. Apart from the sample corroded after 1848 h, the shapes of Bode–phase diagrams were similar at different corrosion time. The peaks of Bode diagram at 1848 h were not obvious at both low–frequency and high–frequency. The low–frequency peak shifted to the left at 1848 h. Generally, the electrochemical impedance spectrum at high frequency reflects the layer corrosion products, and the electrochemical impedance spectrum at low frequency reflects the Faraday process[25–27]. Therefore, it indicated that enhancements of the interfacial reactions process and the anodic dissolution rate at 1848 h[28]. The phase angle peak, which was at high–frequency, gradually declined and moved to a higher frequency range with the prolonged corrosion time except at 0 h, indicating that the corrosion resistance of corrosion product decreased gradually as the corrosion time increased after the samples began to corrode. In the uncorroded sample, the diffusion process was easy because corrosion products were not present on the surface. The phase angle peaks at 1848 h, 504 h and 840 h at low–frequency were small, reflecting that the Faraday processes at these periods were slightly inhibited and the interfacial reactions process was enhanced[26,28].
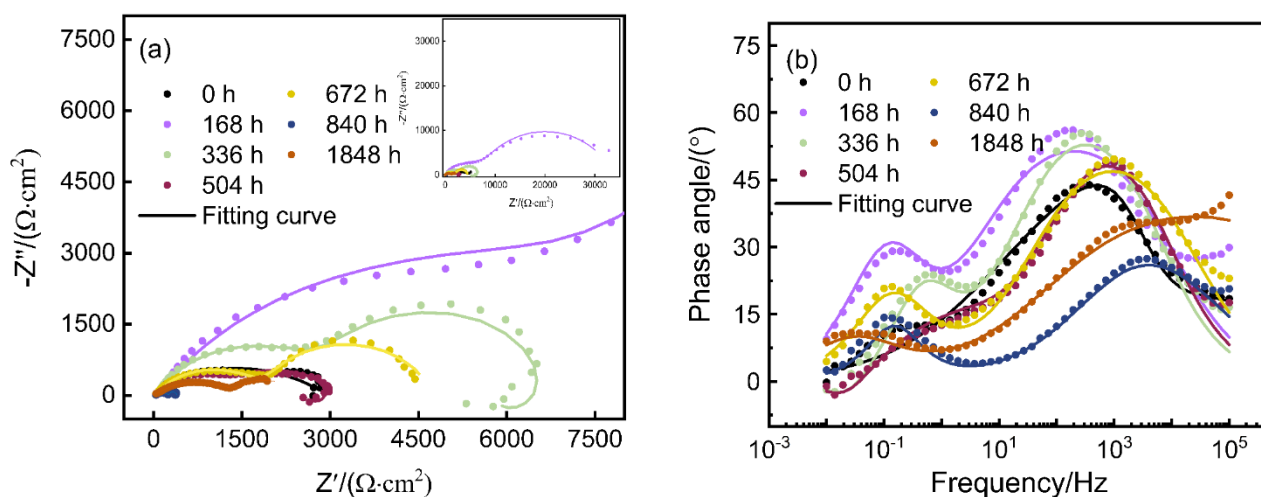

Figure 7. (a) Nyquist diagrams and (b) Bode–phase diagrams of ZAM in the simulated marine atmosphere at different time

The equivalent circuit shown in Fig.8 (a) was used to fit the EIS at 0, 168, 672, 840 and 1848 h. Fig.8 (b) was used to fit the EIS at 336 and 504 h. R_s is the solution resistance. R_r and Q_r are the resistance and capacitance of corrosion product film, respectively. R_L and L are the resistance and inductance. R_{ct} represents the charge transfer resistance and Q_{dl} represents double layer capacitance. The fitting results are shown in Table 3. R_{ct} was higher than or equal to R_r at the early stages, in particular, R_r at 0 h was much less than R_{ct}. It indicated that the process of charge transportation was the rate dominate steps for original ZAM coatings. R_{ct} was smaller than R_r at the latter stage. R_{ct} and R_r both started to increase at 168 h and 672 h compared with the previous stage, and the trend was consistent with that of the corrosion

rate decline at 168–336 h and 672–840 h. And R_r was larger than R_{ct} at 840 h and 1848 h, mainly because the amounts of corrosion products increased with corrosion and the formation of a compact corrosion product made the diffusion difficult.

From our perspective, the sum of the charge transfer resistance R_{ct} and the corrosion product resistance R_r can be typically considered as the polarization resistance R_p^* (* is for distinguishing R_p), R_p^* is provided in Table 3. The result of $1/R_p^*$ reflected corrosion rate which was also consistent with the regulation of the corrosion rate. Therefore, the results of electrochemical measurements in this study were reliable. The corrosion of ZAM exposed to the simulated marine atmosphere would slow down as its exposure to the atmosphere continued according to the electrochemical results of 1848 h.
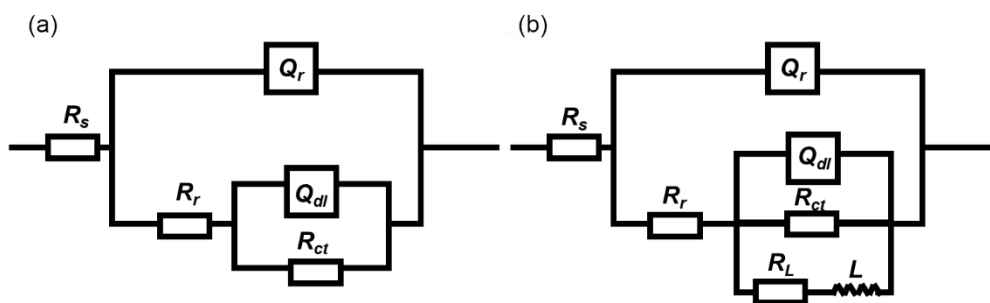

Figure 8. Equivalent circuit used to fit the experimental EIS data of ZAM in the simulated marine atmosphere (a) 0, 168, 672, 840, 1848 h and (b) 336, 504 h

Table 3. Impedance parameters of ZAM after being fitted

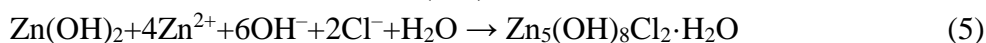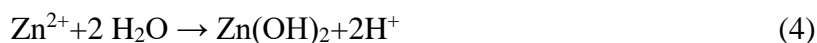|	R_S ($\Omega \cdot cm^2$)	Q_r		R_r ($\Omega \cdot cm^2$)	Q_{dl}		R_{ct} ($\Omega \cdot cm^2$)	R_L ($\Omega \cdot cm^2$)	L ($H \cdot cm^2$)	Chi–squared	$R_p^* (R_r+R_{ct})$ ($\Omega \cdot cm^2$)
		y_r ($\Omega^{-1} \cdot cm^{-2} \cdot S^n$)	n_r		y_{dl} ($\Omega^{-1} \cdot cm^{-2} \cdot S^n$)	n_{dl}					
0	2.00E+01	7.71E–05	4.44E–01	1.06E+02	1.34E–06	8.89E–01	2.84E+03	—	—	2.67E–03	2.94E+03
168	3.96E+01	5.85E–06	7.50E–01	4.76E+03	6.60E–05	9.27E–01	5.33E+03	—	—	1.00E–02	1.01E+04
336	4.66E+01	1.09E–05	7.18E–01	1.33E+03	1.38E–04	8.96E–01	3.63E+03	8.52E+03	7.15E+04	4.26E–03	6.84E+03
504	4.19E+01	9.47E–06	7.18E–01	1.33E+03	2.56E–04	5.48E–01	1.91E+03	4.00E+03	3.54E+04	2.59E–03	3.24E+03
672	2.91E+01	1.58E–05	6.45E–01	1.94E+03	6.01E–04	8.12E–01	2.78E+03	—	—	2.40E–03	4.73E+03
840	2.74E+01	5.42E–05	5.41E–01	2.34E+02	9.45E–03	1.00E+00	1.38E+02	—	—	1.975E–03	3.72E+02
1848	5.94E+00	4.34E–05	4.60E–01	1.44E+03	4.17E–03	6.97E–01	9.79E+02	—	—	1.53E–03	2.42E+03

3.5 Corrosion mechanism

Based on the above analysis, the ZAM coated steel underwent different corrosion stages in a simulated marine atmosphere. The schematic diagram of corrosion mechanism was shown as Fig.9. The specific process is as follows:

The corrosion in the eutectic phase was relatively uniform and severe during the first stage of corrosion because no protective corrosion product had been formed. Therefore, the corrosion rate of ZAM coated steel during the initial stage of corrosion was rapid, and the corrosion process was controlled by charge transportation. Next when the coatings were covered by the protective corrosion product $Zn_5(OH)_8Cl_2 \cdot H_2O$[12,22], the corrosion rate declined rapidly as shown in Fig 9 (a). As the

corrosion progressed, the volume of the corrosion product increased, causing it to be discontinuous. Consequently, the binding force between corrosion products and coatings worsened, causing the corrosion product to fall off easily from coating as shown in Fig 9 (b). And R_{ct} at 336 h was the same as the 0 h, indicating the similarity of between the corrosion present in the original coatings and that in the corroded samples at 336 h. It further suggested that the fresh coating was exposed after the corrosion product fell off, resulting in a charge transfer process similar to that which occurred in the original coating.

The local corrosion in the ZAM coatings was quite severe before the complete corrosion product film was formed. The difference in the potential between the eutectic phase and the primary zinc phase was conducive to the formation of micro–batteries and caused the corrosion to localize in the eutectic phase near the primary zinc phase[29]. Corrosion was of two types as shown in Fig.4 (b) and (c): in the C site in Fig.4 (c), the primary zinc phase was covered by a thin eutectic phase, corrosion preferentially occurred on the thin eutectic phase. When the thin eutectic phase was completely corroded, corrosion would continue to go on the large area eutectic phase at a relatively uniform rate. In the B site in Fig.4 (b), the eutectic phase was located among the primary zinc phase, the area of eutectic phase was much smaller than that of the primary zinc phase. In this case, the corrosion went on along with the eutectic phase in longitudinal direction. Large cathodes and small anodes accelerated the corrosion process. This type of corrosion was dangerous, and can easily lead to the local destruction of the coating or even its failure as shown in Fig.4 (b). This phenomenon had been observed in the coatings after they were exposed to the outdoor marine atmosphere for six months, and the coating was damaged by the penetration of the corrosive medium in the steel surface through the pits.[13]. The Corrosion pits easily generated in the eutectic phase in the marine atmosphere during the initial corrosion stage. Thus, pitting corrosion should pay more attention for ZAM exposed in marine environments. Not only corrosion pits appeared but also many corrosion products in pits disappeared at the early stage of exposure for ZAM by Fig.4 (b). The phenomenon can be explained using the local acidification theory of pitting[30]. The pit acted as the anode because of the low oxygen concentration in it, which caused the anodic dissolution of the eutectic phase. The positive charge in the pit increased gradually as the corrosion progressed, which caused a large number of anions Cl^- to migrate into the pit to maintain the electric neutrality. Equation (3) to (5) show the anodic reaction process. The reaction involving OH^- resulted from hydrolysis, which increased the H^+ ion concentration as the reaction continued in the pit. These H^+ would move out of the pit because of the effect of the electric field. $Zn_5(OH)_8Cl_2 \cdot H_2O$ is not stable in acidic environment[12]. Since the pH value declined and the movement of the H^+, $Zn_5(OH)_8Cl_2 \cdot H_2O$ would be dissolved from the pit. Meanwhile, a cathodic reaction occurred at the interface of atmosphere and coatings[13] as shown in Fig 9 (c). The anodes and cathodes are well separated[12,13], which is conducive to the acidification of the anode and the dissolution of corrosion products[31–33].

$$Zn \rightarrow Zn^{2+} + 2e^- \qquad (3)$$
$$Zn^{2+} + 2\,H_2O \rightarrow Zn(OH)_2 + 2H^+ \qquad (4)$$
$$Zn(OH)_2 + 4Zn^{2+} + 6OH^- + 2Cl^- + H_2O \rightarrow Zn_5(OH)_8Cl_2 \cdot H_2O \qquad (5)$$

As shown in Fig.3 (b), the peaks of Zn at 672 h got stronger than those at 504 h abnormally. This phenomenon could be explained that the eutectic phase around the primary zinc phase was corroded and the corrosion product was dissolved, leading to the exposure of the primary zinc phase and the

enhancement of the Zn diffraction peaks. In addition, R_{ct} at 672 h was nearly the same as 0 h, R_r at 672 h was smaller than R_{ct}, but either 840 h or 1848 h was larger than R_{ct}. These phenomena further confirmed that the corrosion preferentially occurred in the eutectic phase near the primary zinc phase and that the corrosion products in the pit were dissolved, causing the fresh coating to be exposed and corroded. The eutectic phase adjacent to the primary zinc phase decreased with corrosion, and corrosion occurred in the large eutectic phase and in the fresh eutectic phase in the pits. Local corrosion was not significant. Therefore, the corrosion rate declined at 672–840 h. The diffusion process was hindered by the increase in the amount of corrosion products, consequently, the diffusion corrosion of ZAM coatings at 840 h and 1848 h was limited.

The pit was filled with corrosion products as the corrosion developed. Next, the pitting corrosion and corrosion product dissolution were repeated. The corrosion current and H^+ transport processes affected pit development[31]. As the corrosion pits expanded, the time available was not sufficient to dissolve the corrosion products, allowing the primary zinc phase to be surrounded by corrosion products and accelerating the corrosion of the primary zinc phase. The corrosion of the other sites was uniform, and the corrosion rate in the eutectic phase was higher than that in the primary zinc phase, some corrosion products fell off and the coatings surface became uneven as shown in Fig.4 (d) and (e). The schematic diagram is shown in Fig 9 (d).
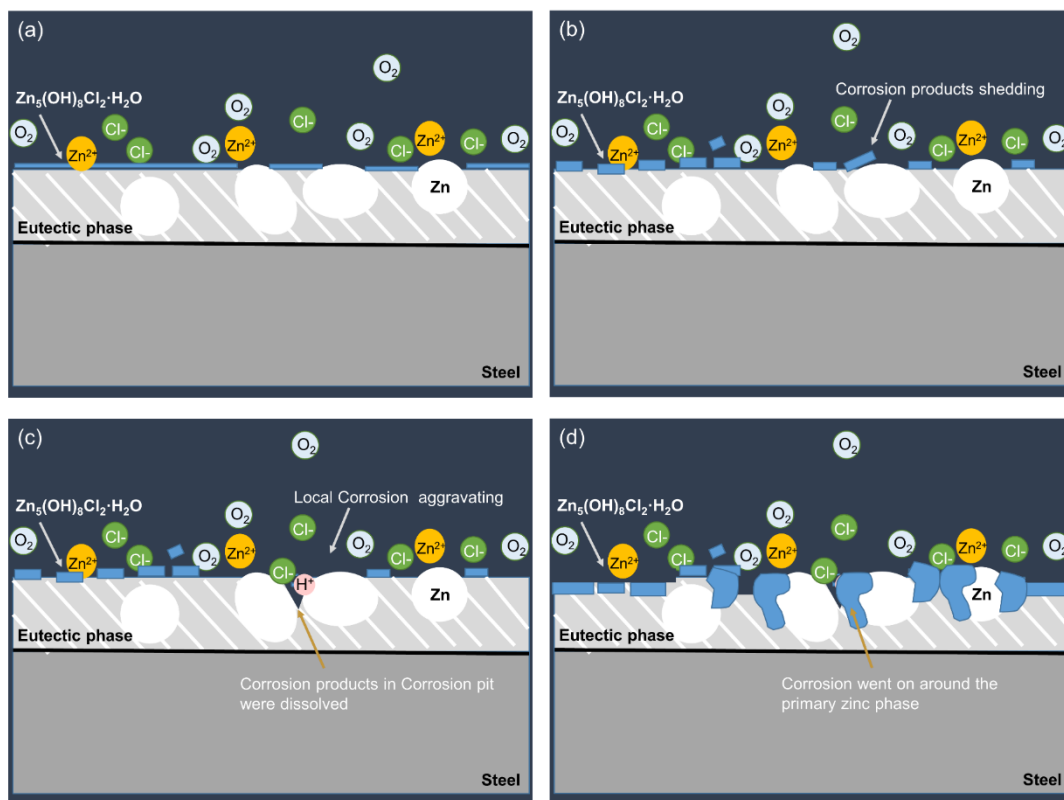

Figure 9. Schematic diagram of corrosion mechanism of ZAM in the simulated marine atmosphere

4. CONCLUSIONS

In this study, the corrosion behavior of ZAM coated steel exposed to a simulated marine atmosphere for 1848 hours was investigated. From the study findings, the following conclusions could be drawn:

(1) The corrosion rate of ZAM coated steel in a simulated marine atmosphere was varied and fluctuated because of the variety of corrosion products during the whole exposure stage. The corrosion process would be slowed down during further exposure as revealed by the electrochemical results.

(2) The corrosion of eutectic phase occurred preferentially which could be divided into two situations, one was large area eutectic phase with relatively uniform corrosion and the other was the smaller area eutectic phase near the primary zinc phase with greater corrosion rate.

(3) Generation and shedding of corrosion products affected the variation of corrosion rate during initial stage, leading to the aggravation of local corrosion and the formation of corrosion pits in the smaller area eutectic phase among the primary zinc phase.

(4) The pH value in corrosion pits decreased during the reaction owing to hydroxide consumption, which led to the dissolution of corrosion products.

References

1. T. Prosek, A. Nazarov, F. Goodwin, J. Šerák and D. Thierry, *Surf. Coat. Technol.,* 306 (2016) 439.
2. T. Prosek, A. Nazarov, A. Le Gac and D. Thierry, *Prog. Org. Coat.,* 83 (2015) 26.
3. N. LeBozec, D. Thierry, A. Peltola, L. Luxem, G. Luckeneder, G. Marchiaro and M. Rohwerder, *Mater. Corros.,* 64 (2013) 969.
4. M. Ahmadi, B. Salgın, B. J. Kooi and Y. Pei, *Mater. Des.,* 186 (2020) 108364.
5. T. Prosek, N. Larche, M. Vlot, F. Goodwin and D. Thierry, *Mater. Corros.,* 61 (2010) 412.
6. D. Thierry, N. LeBozec, A. Le Gac and D. Persson, *Mater. Corros.,* 70 (2019) 2220.
7. J. Sullivan, N. Cooze, C. Gallagher, T. Lewis, T. Prosek and D. Thierry, *Faraday Discuss.,* 180 (2015) 361.
8. J. Sullivan, S. Mehraban and J. Elvins, *Corros. Sci.,* 53 (2011) 2208.
9. D. Persson, T. Prosek, N. LeBozec, D. Thierry and G. Luckeneder, *Corros. Sci.,* 90 (2015) 276.
10. T. Prosek, J. Hagström, D. Persson, N. Fuertes, F. Lindberg, O. Chocholatý, C. Taxén, J. Šerák and D. Thierry, *Corros. Sci.,* 110 (2016) 71.
11. M. Salgueiro Azevedo, C. Allély, K. Ogle and P. Volovitch, *Electrochim. Acta,* 153 (2015) 159.
12. P. Volovitch, T. N. Vu, C. Allély, A. Abdel Aal and K. Ogle, *Corros. Sci.,* 53 (2011) 2437.
13. D. Thierry, D. Persson, G. Luckeneder and K.–H. Stellnberger, *Corros. Sci.,* 148 (2019) 338.
14. X. Lu, Y. Liu, M. Liu and Z. Wang, *J. Mater. Sci. Technol.,* 35 (2019) 1831.
15. K. Bobzin, M. Oete, T. F. Linke and C. Schulz, *Mater. Corros.,* 66 (2015) 520.
16. Y. Liu, A. Ooi, E. Tada and A. Nishikata, *Corros. Sci.,* 147 (2019) 273.
17. T. Prosek, A. Nazarov, U. Bexell, D. Thierry and J. Serak, *Corros. Sci.,* 50 (2008) 2216.
18. N. LeBozec, N. Blandin and D. Thierry, *Mater. Corros.,* 59 (2008) 889.
19. L. Jiang, P. Volovitch, M. Wolpers and K. Ogle, *Corros. Sci.,* 60 (2012) 256.

Int. J. Electrochem. Sci., 17 **(2022)** Article Number: 22054

14

20. S. Schürz, G. H. Luckeneder, M. Fleischanderl, P. Mack, H. Gsaller, A. C. Kneissl and G. Mori, *Corros. Sci.,* 52 (2010) 3271.
21. S. Schuerz, M. Fleischanderl, G. H. Luckeneder, K. Preis, T. Haunschmied, G. Mori and A. C. Kneissl, *Corros. Sci.,* 51 (2009) 2355.
22. N. C. Hosking, M. A. Ström, P. H. Shipway and C. D. Rudd, *Corros. Sci.,* 49 (2007) 3669.
23. P. Volovitch, C. Allely and K. Ogle, *Corros. Sci.,* 51 (2009) 1251.
24. S. Feliu, M. Morcillo and S. Feliu, *Corros. Sci.,* 34 (1993) 415.
25. J. Stoulil, T. Prosek, A. Nazarov, J. Oswald, P. Kriz and D. Thierry, *Mater. Corros.,* 66 (2015) 777.
26. M. Wang, C. Qiao, X. Jiang, L. Hao and X. Liu, *J. Mater. Sci. Technol.,* 51 (2020) 40.
27. E. Barsoukov and R. J. Macdonald, *Impedance Spectroscopy: Theory, Experiment, and Applications*. Wiley–Interscience (2005) Hoboken.
28. C. Qiao, M. Wang, L. Hao, X. Liu, X. Jiang, X. An and D. Li, *J. Mater. Sci. Technol.,* 75 (2021) 252.
29. L. Zheng, F. Cao, W. Liu, B. Jia and J. Zhang, *Acta Metall. Sin. (Engl. Lett.).,* 23 (2010) 416.
30. M. G. Alvarez and J. R. Galvele, *Corrosion,* 32 (1976) 285.
31. I. S. Cole, W. D. Ganther, S. A. Furman, T. H. Muster and A. K. Neufeld, *Corros. Sci.,* 52 (2010) 848.
32. T. H. Muster, W. D. Ganther and I. S. Cole, *Corros. Sci.,* 49 (2007) 2037.
33. A. D. Keitelman, S. M. Gravano and J. R. J. C. S. Galvele, *Corros. Sci.,* 24 (1984) 535.